Nearly Simultaneous Optical, Ultraviolet, and X-ray Observations of Three PG Quasars

Gerard A. Kriss
Department of Physics and Astronomy
The Johns Hopkins University
Baltimore, MD 21218

Abstract

We present nearly simultaneous optical, ultraviolet, and X-ray observations of three low redshift quasars. The EXOSAT X-ray spectra span the range of observed spectral indices for quasars from the canonical 0.7 energy index typical of Seyfert galaxies for PG0923+129 (Mrk 705) to the steep spectral indices frequently seen in higher luminosity quasars with an index of 1.58 for PG0844+349 (Ton 951). None of the quasars exhibits any evidence for a soft X-ray excess. This is consistent with accretion disk spectra fit to the IR through UV continua of the quasars — the best fitting disk spectra peak at ~6 eV with black hole masses in the range 5×10^7 $M_\odot$ to 1×10^9 $M_\odot$ and mass accretion rates of ~0.1 times the Eddington-limited rate. These rather soft disk spectra are also compatible with the observed optical and ultraviolet line ratios.

Final Technical Report submitted to NASA for Grant NAG8-562.

Gerard A. Kriss

Dr. Gerard A. Kriss
Principal Investigator
March 8, 1990

I. Introduction

The continuum radiation of quasars spans many decades in frequency, and it has become increasingly clear that a proper understanding of the radiation mechanisms powering the central source in quasars requires observations in many wavebands. In the near IR and optical bands, a power law of index ~ -1 dominates the continuum (Rieke 1978; Malkan and Sargent 1982; Neugebauer *et al.* 1987). This power law often extrapolates well to the X-ray at 2 keV (Malkan and Sargent 1982; Elvis *et al.* 1986; Ward *et al.* 1987). The X-ray continuum again is a power law. Most Seyfert 1 galaxies have spectral indices of ~ -0.7 (Mushotzky 1984), but spectral indices for quasars range from -0.5 to -2.2 (Elvis, Wilkes, and Tananbaum 1985; Elvis *et al.* 1986; Wilkes and Elvis 1987). Superposed on these underlying power law continua is a broad excess of emission in the blue and ultraviolet (the "blue bump") that may be thermal radiation from an accretion disk around a black hole (Malkan and Sargent 1982; Malkan 1983). This broad excess may continue through the extreme ultraviolet range into the soft X-ray band to link the "blue bump" with the soft X-ray excesses seen in many objects (the "big bump": Elvis and Lawrence 1985; Bechtold *et al.* 1987). In many AGN, particularly quasars and Seyfert 1 galaxies, these power law continua and the "big bump" dominate the energy budget of the active nucleus.

Strong correlations exist between various wavebands as indicated by broad band studies of large samples of quasars and active galaxies (Kriss and Canizares 1985; Avni and Tananbaum 1986; Ward *et al.* 1987; Worrall *et al.* 1987; Worrall 1987; Kriss 1988), yet it is unclear what properties of the underlying radiation mechanisms are reflected in these correlations. Current opinion favors accretion onto a black hole as the source for the energetic output because of its high efficiency. Since it is highly unlikely that the inflow is perfectly spherical, the accreting material probably forms a viscous disk (Shakura and Sunyaev 1973) to shed the angular momentum before disappearing beyond the event horizon. The UV and optical continua of many quasars and Seyfert 1 galaxies have energy distributions characteristic of the expected disk radiation (Malkan and Sargent 1982; Malkan 1983; Sun and Malkan 1989), but the peak of the disk spectrum associated with supermassive black holes of 10^7 to 10^9 M_O lies in the unobservable extreme ultraviolet.

Galactic absorption hampers our view of the EUV at low redshifts, and absorption in the inter-galactic medium is problematic at higher redshifts. Inference of the shape of the EUV continuum using the broad emission lines photoionized by this continuum as probes is the only method currently available. Several combinations of prominent UV and optical emission lines are sensitive to different portions of the ionizing continuum from the UV through the X-ray band (Krolik and Kallman 1988). Since active galaxies and quasars can undergo continuum luminosity variations of factors of two or more on time scales of weeks to months (Tennant and Mushotzky 1983; Zamorani *et al.* 1984; Clavel *et al.* 1990), however, it is important to obtain nearly simultaneous observations of the optical, UV, and X-ray bands to construct a self-consistent model of the entire spectrum.

Few AGN have been observed simultaneously in all three wavebands. The best studies to date include observations of NGC 4151 (Perola *et al.* 1982; Perola *et al.* 1986), Fairall 9 (Morini *et al.* 1986), and 3C 273 (Courvoisier *et al.* 1987). In this paper, we present near-

simultaneous optical, ultraviolet, and X-ray observations of three PG quasars. Combining these data with published IR measurements, we model the IR through X-ray continua with power laws plus an accretion disk spectrum. The EUV portion of the disk spectrum is constrained by the ratios of the broad emission lines in our optical and UV spectra. The observations are presented in section II, the disk models are discussed in section III, and we conclude with a discussion of the IR through X-ray spectral energy distribution of quasars in section IV.

II. The Coordinated Observations

The objects of our study, PG0844+349 (Ton 951), PG0923+129 (Mrk 705), and PG1229+204 (Ton 1542), were chosen as quasars in the PG catalogue (Schmidt and Green 1983) brighter than $m_B = 14.5$ that have not been previously studied in great detail. We also chose redshifts greater than 0.015 to prevent geocoronal Ly α contamination of the quasar Ly α, and redshifts less than 0.17 to keep C IV λ1549 within the IUE short wavelength bandpass.

Our observing strategy was to obtain all observations for a given object within a time span of one month. All of our objects are radio-quiet, and show only low amplitude variability on one month time scales. Our ground-based optical observations offered the most flexibility in scheduling, and so we made several observations of each object bracketing the UV and X-ray observations to guard against any large changes in luminosity. One quasar (PG1229+204) was not observed with IUE since extensive observations of it are available in the IUE archives.

A summary of our new observations of these three quasars is presented in Table 1 where we give the name of each quasar, its redshift, the UT date of each observation, the exposure time, and the instrument used for the observation. Details of the observations are presented in the following sub-sections.

a) Optical Spectrophotometry

Since nearly simultaneous observations at optical, UV, and X-ray wavelengths are extremely difficult to schedule, we obtained optical observations at dates both before and after the UV and X-ray observations. This permits us to check after the fact that there were no gross changes in source luminosity on time scales of a month or more.

Observations with the McGraw-Hill 1.3m telescope[1] (MGH 1.3m) used the photon-counting, intensified-Reticon spectrometer (Shectman and Hiltner 1976).

---

[1]The McGraw-Hill Observatory is operated by the University of Michigan, the Massachusetts Institute of Technology, and Dartmouth College.

The spectra cover the wavelength range 4000 to 7000 Å with a resolution of ~12 Å. A circular aperture of 5.6 arc seconds gave consistent fluxes on observations of program objects interspersed with standard stars. At least three white dwarf standards were observed each night. The raw spectra were sky-subtracted and flat-fielded with exposures of an internal tungsten lamp. They were then placed on a linear wavelength scale using exposures of

Table 1

OBSERVING LOG

Name	z	Date (UT)	Exposure (sec)	Instrument
PG0844+349 (Ton 951)	0.064	25.201 Mar 1985	900	Lick 3m
		21.578 Apr 1985	2098	EXOSAT - Lexan
		21.611 Apr 1985	8193	EXOSAT - Boron
		21.713 Apr 1985	4377	EXOSAT - Al/P
		1.594 May 1985	2100	IUE - SWP25827
		21.174 May 1985	1800	MGH 1.3m
		22.181 May 1985	600	MGH 1.3m
PG0923+129 (Mrk 705)	0.029	25.305 Mar 1985	900	Lick 3m
		1.332 May 1985	6000	IUE - SWP25826
		9.023 May 1985	3139	EXOSAT - Lexan
		9.064 May 1985	6574	EXOSAT - Al/P
		9.150 May 1985	11652	EXOSAT - Boron
		22.158 May 1985	960	MGH 1.3m
PG1229+204 (Ton1542)	0.064	25.601 Mar 1985	900	Lick 3m
		21.240 May 1985	2160	MGH 1.3m
		22.218 May 1985	900	MGH 1.3m
		8.083 Jun 1985	4250	EXOSAT - Lexan
		8.120 Jun 1985	11197	EXOSAT - Al/P
		8.216 Jun 1985	21202	EXOSAT - Boron
		8.735 Jun 1985	2829	EXOSAT - Lexan
		1.194 Jul 1985	600	MGH 1.3m

internal Hg, Ne, and A lamps. Flux calibration curves obtained from each standard observation show agreement to better than 10% in all cases. A mean calibration curve derived each night was used to flux calibrate the object spectra. Figure 1 shows the optical spectra obtained for each observed quasar.

Fluxes of prominent emission lines were obtained by fitting a multicomponent model to small regions of the spectra. This permits the strong multiplets of Fe II to be deblended from Hγ, He II λ4686, Hβ and [O III] $\lambda\lambda$4959, 5007. The continuum spectrum is linearly interpolated between points on either side of the line complex selected by the user, and Gaussian line profiles are fit to the strong emission lines. The Fe II lines are presumed to have relative strengths as given by Phillips (1978) and velocity widths the same as for Hβ. Table 2 summarizes the measured line fluxes and measurement errors.

b) IUE Observations

Table 2

FLUXES OF PROMINENT OPTICAL AND UV EMISSION LINES

Line	PG0844+349 (10^{-13} erg cm^{-2}s^{-1})	PG0923+129 (10^{-13} erg cm^{-2}s^{-1})	PG1229+204 (10^{-13} erg cm^{-2}s^{-1})
[S II] λλ6716,6732	...	...	0.32±0.10
Hα	11.0±0.8	7.4±0.3	9.3±0.8
He I λ5876	0.88±0.25	0.61±0.15	0.93±0.30
Fe II Red	2.52±0.5	0.80±0.20	1.20±0.20
[O III] λ5007	1.0±0.1	1.1±0.1	0.65±0.05
[O III] λ4959	0.33±0.07	0.39±0.05	0.20±0.05
Hβ	3.6±0.2	1.7±0.2	2.8±0.25
He II λ4686	<0.13	<0.09	<0.05
Fe II Blue	3.5±0.5	1.2±0.25	1.9±0.3
Hγ	2.7±0.4	0.83±0.12	1.4±0.2
Hδ	0.80±0.1	0.58±0.1	0.54±0.15
Hε	0.62±0.15	0.39±0.15	0.38±0.1
He I λ3889	<0.38	0.48±0.10	0.35±0.10
Mg II λ2798	...	...	4.0±0.3
C III] λ1909	...	...	2.5±0.5
He II λ1640	<0.6	1.0±0.5	<0.6
C IV λ1549	5.7±1.0	15.6±1.0	13.7±1.0
N V λ1240	2.6±1.0	4.5±1.0	2.6±0.5
Ly α	20.0±1.0	16.5±1.0	32.4±1.1

The two IUE observations were made with the SWP camera in low resolution mode using the large aperture (see Boggess *et al.* 1978 for a description of the IUE instruments). The targets were acquired using blind offsets from nearby SAO stars. The data were processed and the spectra extracted using the 1979 November version of IUESIPS. Short and long wavelength UV spectra of the quasar PG1229+204 were obtained from the IUE archives. The short wavelength spectra of the three quasars are shown in Figure 2. Fluxes of the prominent UV and emission lines observed in the three quasars are also presented in Table 2. These were determined interactively. Continuum points were selected on either side of the emission line, and the net flux in the spectrum above the continuum between those points was calculated.

c) EXOSAT Observations

Each quasar in our program was observed with both the Medium Energy experiment (ME) and the Low Energy telescope (LE) on the EXOSAT Observatory. Descriptions of

these instruments can be found in Taylor *et al.* (1981). The ME observed each target with half the detector array offset on background sky. The halves observing the target and sky were swapped halfway through each observation for good background subtraction. The LE was used with the Channel Multiplier Array (CMA) detector and several broad band filters. We first used the highest throughput filter (#6, thin Lexan) to estimate the source flux. We then made additional observations with filters 2 (Aluminium/Paralene) and 4 (Boron) to crudely measure the soft X-ray spectrum. A final observation with the thin Lexan filter was made to check on source variability.

The ME data and the LE data through the separate filters were simultaneously fit with a power law spectrum with low energy galactic absorption. The quasars PG0923+129 and PG1229+204 were sufficiently bright and the observations were sufficiently long that good constraints can be placed on both the spectral index and the neutral hydrogen column density in the spectral fits. Since PG0844+349 was so weak, we have also evaluated the fits with the galactic column density fixed at $N_H = 3.9 \times 10^{20}$ cm^{-2}, the value given by Burstein and Heiles (1978). The best fit parameters for each source with 90% confidence limits are given in Table 3, and the best fit X-ray spectra are shown in Figures 3, 4, and 5. While PG0844+349 and PG1229+204 have steep X-ray spectra, these steep spectra extend into the highest energy channels of the ME. None of the three quasars show any evidence of excess flux above the fitted power law in the low energy filters of the LE observations.

Table 3

X-RAY FLUXES AND BEST FIT SPECTRAL PARAMETERS

Object	2-6 keV Flux (10^{-12} erg cm^{-2}s^{-1})	F_{2keV} (μJy)	α	N_H (atoms cm^{-2})
PG0844+349	1.3	0.68	$1.58^{+1.93}_{-0.29}$	$3.0^{+5.3}_{-2.83}$
PG0844+349	1.3	0.68	$1.72^{+0.44}_{-0.24}$	3.9 (Fixed)
PG0923+129	7.4	1.0	$0.72^{+0.37}_{-0.31}$	$2.3^{+3.9}_{-1.7}$
PG1229+204	2.4	0.62	$1.48^{+0.21}_{-0.07}$	$1.60^{+0.86}_{-0.72}$

III. The IR through X-ray Continua

We have combined our new observations with published IR photometry from Neugebauer *et al.* (1987) to form a complete picture of the luminous continuum from infrared to X-ray wavelengths. Following the standard procedure of Malkan (1983) and Sun and Malkan (1989), we fit a multi-component model to the continuum data consisting of an IR-optical power law, starlight in the optical and near IR, Balmer continuum emission in the near UV, and an accretion disk spectrum which dominates the UV continuum. Our initial

fits are done without any constraints imposed by the X-ray data or the UV and optical emission line ratios. We then test our best fit models against these additional constraints.

The continuum data points with 1σ error bars are given in Table 4. The best fitting models are illustrated with the data points for PG0844+349 and PG1229+204 in Figure 6.

The most significant constraints on the shape of the disk spectrum in the extreme UV are set by the lack of a soft X-ray excess in any of the three quasars and by the ratio of the He II lines to the flux in Ly α. The disk spectrum must peak at $<<100$ eV to avoid a significant contribution to the soft X-ray LE data. The He II lines are formed almost entirely through recombination (MacAlpine 1981; Krolik and Kallman 1988), and so they simply count photons beyond the He II ionization edge at 54.4 eV. To use this as a spectral constraint, one either needs an accurate measure of the covering fraction of the broad line clouds, or an additional line to count photons at lower energies in the Lyman continuum. The best candidate line is Ly α. A significant fraction of the luminosity in Ly α comes from processes other than recombination, so it is not a perfect photon counter. However, over the range of physical conditions studied by Krolik and Kallman (1988), the ratio of Ly α photons to Lyman continuum photons varies only by a factor of two. For disk spectra that peak around 10 eV plus a $\nu^{-1.1}$ power law, they find He II λ1640 / Ly α ratios of $\sim$0.02, while disks of 80 eV have ratios of 0.06 - 0.11.

We do not detect He II λ1640 in the UV spectra of any of the three quasars. We can set significant upper limits, however, as our data in Table 2 show. The ratio of these upper limits to Ly α constrain the disk temperature at the peak to be $<$6.0 eV for PG0844+349, $<$6.9 eV for PG0923+129, and $<$5.7 eV for PG1229+204. These values are all compatible with our best fits to the optical and UV continuum, and they are low enough to ensure there is no significant contribution to the soft X-ray flux.

In Table 5 we give the parameters of our best fits to the quasars. Black hole masses range from $\sim 5 \times 10^7\ M_\odot$ to $1 \times 10^9\ M_\odot$, and mass accretion rates are $\sim$0.1 of the Eddington-limited rate, similar to those of other quasars in the study of Sun and Malkan (1989).

IV. Discussion

Understanding how, or if, the various components of the quasar continuum are related can provide direct clues to the energy generation process. While the optical-IR power law extrapolates well to the X-ray at 2 keV, particularly in low redshift, low luminosity AGN (Malkan and Sargent 1982; Malkan 1984; Elvis *et al* 1986), there is a significant tendency for the X-ray continuum to grow fainter relative to the optical in high redshift, high luminosity quasars (Kriss 1988) such that $L_{2\ keV} \sim L_{1\mu m}^{0.7}$. This is the same as the relation seen between the optical/UV continuum at 2500 Å and the X-ray continuum (Kriss and Canizares 1985; Avni and Tananbaum 1986; Kriss 1988). This suggests a more direct connection between the optical-IR power law and the thermal accretion disk than between the X-ray power law and either component.

More than one process may be contributing to the X-ray power law as well. Wilkes and Elvis (1987) find that radio-loud AGN tend to have flatter X-ray spectra than radio-

Table 4

IR THROUGH X-RAY CONTINUUM DATA

PG0844+349			PG0923+129			PG1229+204		
log ν (Hz)	log νF_ν (erg cm^{-2}s^{-1})	Error	log ν (Hz)	log νF_ν (erg cm^{-2}s^{-1})	Error	log ν (Hz)	log νF_ν (erg cm^{-2}s^{-1})	Error
13.47	-10.83	-11.66	13.91	-10.67	-11.67	13.47	-10.86	-11.55
13.91	-10.81	-11.82	14.13	-10.62	-11.78	13.91	-10.71	-11.73
14.13	-10.77	-11.91	14.26	-10.57	-11.73	14.13	-10.75	-11.89
14.26	-10.76	-11.90	14.37	-10.57	-11.73	14.26	-10.81	-11.95
14.37	-10.72	-11.87	14.62	-10.59	-11.59	14.37	-10.85	-11.99
14.60	-10.57	-11.57	14.70	-10.68	-11.68	14.60	-10.74	-11.74
14.66	-10.56	-11.56	14.74	-10.70	-11.70	14.66	-10.74	-11.74
14.73	-10.58	-11.58	14.79	-10.77	-11.77	14.73	-10.75	-11.74
14.82	-10.55	-11.55	14.85	-10.82	-11.82	14.82	-10.71	-11.74
14.89	-10.35	-11.35	14.90	-10.75	-11.75	14.89	-10.52	-11.74
15.23	-10.57	-11.29	15.23	-10.62	-11.44	15.00	-10.52	-11.13
15.31	-10.60	-10.91	15.31	-10.61	-11.20	15.01	-10.54	-11.27
15.35	-10.67	-11.05	15.35	-10.69	-11.29	15.05	-10.57	-11.62
15.41	-10.59	-11.13	17.08	-11.51	-12.36	15.08	-10.55	-11.66
17.08	-11.45	-12.26	17.22	-11.42	-12.27	15.09	-10.51	-11.51
17.22	-11.51	-12.26	17.33	-11.46	-11.97	15.12	-10.60	-11.43
17.33	-11.59	-11.98	17.53	-11.22	-11.67	15.14	-10.65	-11.30
17.70	-11.49	-11.97	17.66	-11.33	-11.96	15.17	-10.55	-11.33
17.78	-11.67	-11.95	17.76	-11.22	-11.95	15.23	-10.45	-11.42
17.92	-12.02	-11.87	17.84	-11.24	-11.94	15.31	-10.43	-11.17
			17.91	-11.22	-11.89	15.35	-10.44	-11.36
			17.97	-11.09	-11.83	15.40	-10.29	-11.08
			18.03	-11.09	-11.74	17.08	-11.32	-12.37
			18.08	-11.36	-11.86	17.22	-11.35	-12.43
			18.12	-10.97	-11.53	17.33	-11.42	-12.43
			18.17	-11.19	-11.39	17.42	-11.46	-12.49
						17.49	-11.57	-12.20
						17.53	-11.61	-12.45
						17.71	-11.54	-12.41
						17.80	-11.60	-12.42
						17.87	-11.66	-12.41
						17.94	-11.68	-12.37
						18.00	-11.71	-12.30
						18.05	-11.65	-12.19
						18.10	-11.90	-12.08
						18.14	-11.99	-11.98

Table 5

ACCRETION DISK FITS

Object	α	Mass ($M_\odot$)	$\dot{M}$ ($\dot{M}_{Eddington}$)	T_{disk} (eV)
PG0844+349	-1.23	1.0×10^9	0.06	5.2
PG0923+129	-1.25	5.0×10^7	0.10	4.6
PG1229+204	-1.21	6.9×10^7	0.15	5.1

quiet objects. They suggest that the steeper spectra with indices of ~ -1 found in the radio quiet quasars are related to the optical-IR power law, and that the flatter spectra seen in radio-loud quasars is an additional component due to inverse Compton scattering of the radio continuum.

Many Seyfert 1 galaxies and low redshift quasars exhibit a "soft X-ray excess" above the usual power law. Some examples include 1E1426+015 (Reichert *et al.* 1982), NGC 4051 (Lawrence *et al.* 1985), and Mrk 335 (Pounds *et al.* 1986; Turner and Pounds 1987). The classic object with a soft X-ray excess is PG1211+143, which has a spectral index of -2.2 in the *Einstein* Imaging Proportional Counter (Elvis, Wilkes, and Tananbaum 1985). If this soft excess is the high energy tail of the thermal accretion disk spectrum, then this "big bump" dominates the energy output of these objects.

Geometrically thin disk models (e.g., Malkan 1983) have difficulties connecting the UV bump to the soft X-ray excess (Bechtold *et al.* 1987). Disks hot enough to make the connection have small black hole masses, and so require super-Eddington accretion rates to produce enough luminosity. This will invariably puff up the disk and render the thin disk approximation invalid. If the accretion disk spectrum is Comptonized by a hot corona, however, this could explain both the "blue bump" and the soft X-ray excess with a single component (Czerny and Elvis 1987). More recent thin disk models by Sun and Malkan (1989) which take into account general relativistic effects and the inclination of the disk relative to the observer can also produce enough high energy flux to link the blue bump to the soft X-ray excess in a single "big bump".

None of the quasars observed in our program show soft X-ray excesses. If the soft X-ray excess is linked to the EUV portion of the disk spectrum, this is consistent with our observations — the observed line ratios in PG0844+349, PG0923+129, and PG1229+204 do not require much flux beyond the He II ionization edge at 54.4 eV. In contrast, the classic "big bump" quasar PG1211+143 has an unusually high ratio of He II λ1640 to Ly α of 0.106. This is consistent with a disk spectrum that peaks at 80 eV in the photoionization models of Kallman and Krolik (1988). Other AGN which also exhibit soft X-ray excesses

also have high values of He II λ1640 / Ly α (Kriss 1990). This suggests that soft X-ray excesses may well be linked to the high energy tail of the disk spectrum, and that UV and optical spectra obtained simultaneously with X-ray spectral observations may place significant constraints on the shape of the disk spectrum in the extreme ultraviolet.

This work was supported in part by NASA Grant NAG8-562.

References

Avni, Y., and Tananbaum, H. 1986, *Ap. J.*, **305**, 83.

Bechtold, J., Czerny, B., Elvis, M., Fabbiano, G., and Green, R. F. 1987, *Ap.J.*, **314**, 699.

Boggess, A. *et al.* 1978, *Nature*, **275**, 372.

Burstein, D., and Heiles, C. 1978, *Ap. J.*, **225**, 40.

Clavel, J., *et al.* 1990, *Ap.J.*, in press.

Courvoisier, T. J.-L., *et al.* 1987, *Astr. Ap.*, **176**, 197.

Czerny, B., and Elvis, M. 1987, *Ap.J.*, **321**, 305.

Elvis, M. *et al.* 1986, *Ap.J.*, **310**, 291.

Elvis, M., and Lawrence, A. 1985, in *Proceedings of the Seventh Santa Cruz Summer Workshop on Astronomy and Astrophysics*, ed. J. S. Miller.

Elvis, M., Wilkes, B. J., and Czerny, B. 1986, in *The Physics of Accretion onto Compact Objects*, eds. K. O. Mason, M. G. Watson, and N. White (Springer Verlag), in press.

Elvis, M., Wilkes, B., and Tananbaum, H. 1985, *Ap.J.*, **292**, 357.

Kriss, G. A. 1988, *Ap. J.*, **397**, 177.

Kriss, G. A. 1990, in preparation.

Kriss, G. A., and Canizares, C. R. 1985, *Ap. J.*, **297**, 177.

Krolik, J. H., and Kallman, T. R. 1988, *Ap.J.*, **324**, 714.

Lawrence, A. Watson, M. G., Pounds, K. A., and Elvis, M. 1985, *M.N.R.A.S.*, **217**, 685.

MacAlpine, G. M. 1981, *Ap.J.*, **251**, 465.

Malkan, M. A. 1983, *Ap.J.*, **268**, 582.

Malkan, M. A., and Sargent, W. L. W. 1982, *Ap.J.*, **254**, 22.

Morini, M., Chiapetti, L., Maccagni, D., Maraschi, L., Molteni, D., Tanzi, E. G., Treves, A., and Wolter, A. 1986, *Ap.J. (Letters)*, **306**, L71.

Mushotzky, R. F. 1984, *Advances in Space Research*, **3**, 157.

Neugebauer, G., Green, R. J., Matthews, K., Schmidt, M., Soifer, B. T., and Bennett, J. 1987, *Ap.J.(Supplement)*, **63**, 615.

Perola, G. C., *et al.* 1982, *M.N.R.A.S.*, **200**, 293.

Perola, G. C., *et al.* 1986, *Ap.J.*, **306**, 508.

Phillips, M. M. 1978, *Ap.J. (Supplement)*, **38**, 187.

Pounds, K. A., Warwick, R. S., Culhane, J. L., and deKorte, P. A., J. 1986, *M.N.R.A.S.*, **218**, 685.

Reichert, G. A., Mason, K. O., Thorstensen, J. R., and Bowyer, S. 1982, *Ap.J.*, **260**, 437.

Rieke, G. 1978, *Ap.J.*, **250**, 87.

Schmidt, M., and Green, R. F. 1983, *Ap.J.*, **269**, 352.

Shakura, N. I., and Sunyaev, R. A. 1973, *Astr.Ap.*, **24**, 337.

Shectman, S. A., and Hiltner, W. A. 1976, *Pub.A.S.P.*, **88**, 960.

Sun, W.-H., and Malkan, M. A. 1989, *Ap.J.*, **346**, 68.

Turner, T. E., and Pounds, K. A. 1987, *M.N.R.A.S.*, **224**, 443.

Tananbaum, H., Avni, Y., Green, R. F., Schmidt, M., and Zamorani, G. 1986, *Ap. J.*, **305**, 57.

Taylor, B. G., Andresen, R. D., Peacock, A., and Zoble, R. 1981, *Space Sci. Rev.*, **30**, 479.

Tennant, A. F., and Mushotzky, R. F. 1983, *Ap.J.*, **264**, 92.

Ward, M., Elvis, M., Fabbiano, G., Carleton, N. P., Willner, S. P., and Lawrence, A. 1987, *Ap.J.*, **315**, 74.

Wilkes, B. J., and Elvis, M. 1987, *Ap.J.*, **323**, 243.

Worrall, D. M. 1987, *Ap.J.*, **318**, 188.

Worrall, D., Giommi, P., Tananbaum, H., and Zamorani, G. 1987, *Ap. J.*, **313**, 596.

Zamorani, G., Giommi, P., Maccacaro, T., and Tananbaum, H. 1984, *Ap. J.*, **278**, 28.

Figure Captions

Figure 1 - Panels (a), (b), and (c) illustrate the 4000 to 7000 Å optical spectra of the quasars PG0844+349, PG0923+129, and PG1229+204 respectively. Fluxes are in erg cm^{-2} s^{-1}.

Figure 2 - Panels (a), (b), and (c) illustrate the 1200 to 2000 Å ultraviolet spectra of the quasars PG0844+349, PG0923+129, and PG1229+204 respectively. Fluxes are in erg cm^{-2} s^{-1}.

Figure 3 - The X-ray spectrum of PG0844+349 obtained with the ME and LE experiments of the EXOSAT Observatory. The ordinate is in units of counts s^{-1} $detector^{-1}$, where "detector" represents an independent energy channel of the ME or a particular filter selection for the LE. The abscissa is in keV. Vertical error bars are 1 and the horizontal bars illustrate the width in energy of each channel for the ME, or the effective bandpass of the filter used with the CMA on the LE telescope.

Figure 4 - The X-ray spectrum of PG0923+129 obtained with the ME and LE experiments of the EXOSAT Observatory. The ordinate is in units of counts s^{-1} $detector^{-1}$, where "detector" represents an independent energy channel of the ME or a particular filter selection for the LE. The abscissa is in keV. Vertical error bars are 1 and the horizontal bars illustrate the width in energy of each channel for the ME, or the effective bandpass of the filter used with the CMA on the LE telescope.

Figure 5 - The X-ray spectrum of PG1229+204 obtained with the ME and LE experiments of the EXOSAT Observatory. The ordinate is in units of counts s^{-1} $detector^{-1}$, where "detector" represents an independent energy channel of the ME or a particular filter selection for the LE. The abscissa is in keV. Vertical error bars are 1 and the horizontal bars illustrate the width in energy of each channel for the ME, or the effective bandpass of the filter used with the CMA on the LE telescope.

Figure 6 - The IR to X-ray continuum of the quasars PG0844+349 and PG1229+204 are shown. Continuum data points with error bars are shown as crosses, and the best fitting accretion disk plus optical power law model is shown as a solid line.

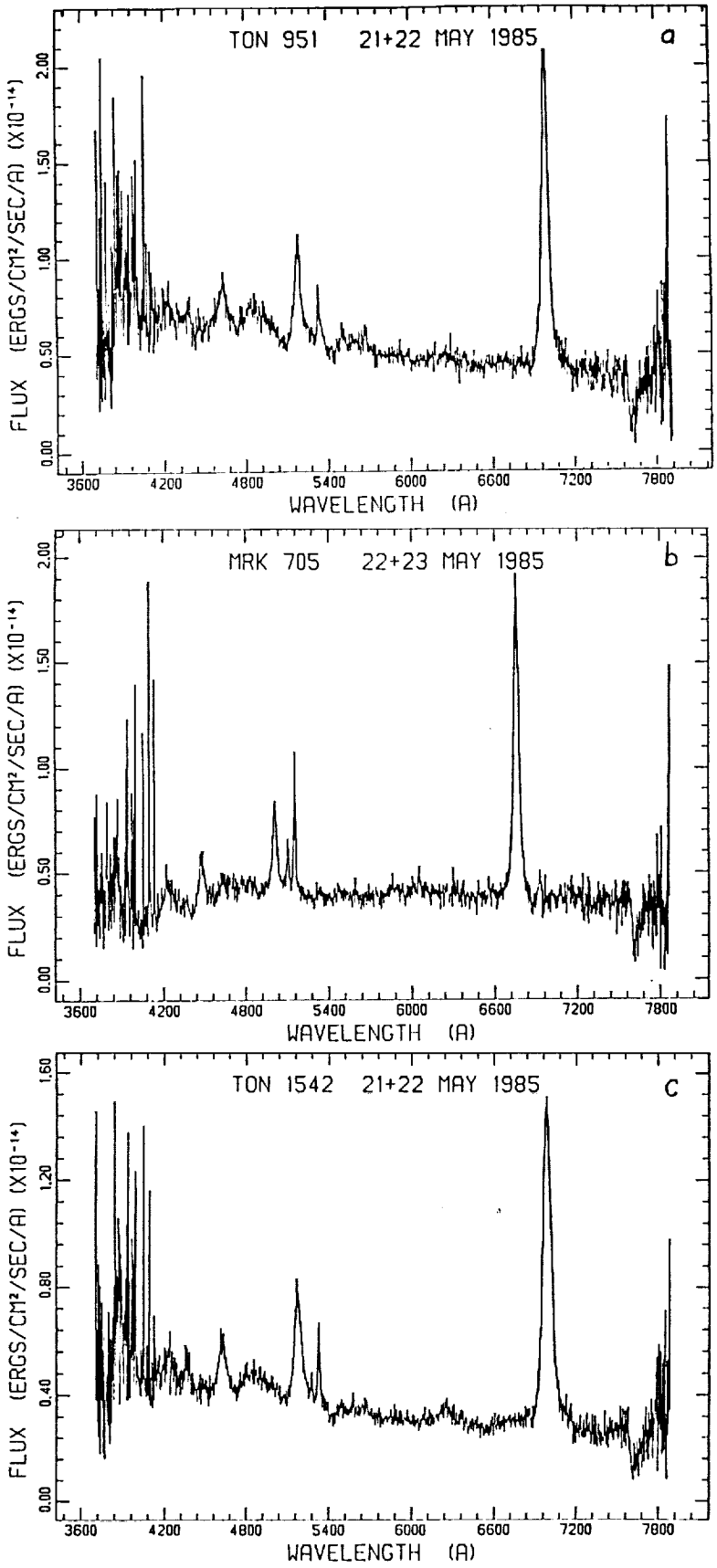
TON 951 21+22 MAY 1985
a
FLUX (ERGS/CM²/SEC/A) (X10⁻¹⁴)
0.00
0.50
1.00
1.50
2.00
3600
4200
4800
5400
6000
6600
7200
7800
WAVELENGTH (A)
MRK 705 22+23 MAY 1985
b
FLUX (ERGS/CM²/SEC/A) (X10⁻¹⁴)
0.00
0.50
1.00
1.50
2.00
3600
4200
4800
5400
6000
6600
7200
7800
WAVELENGTH (A)
TON 1542 21+22 MAY 1985
c
FLUX (ERGS/CM²/SEC/A) (X10⁻¹⁴)
0.00
0.40
0.80
1.20
1.60
3600
4200
4800
5400
6000
6600
7200
7800
WAVELENGTH (A)

Figure 1

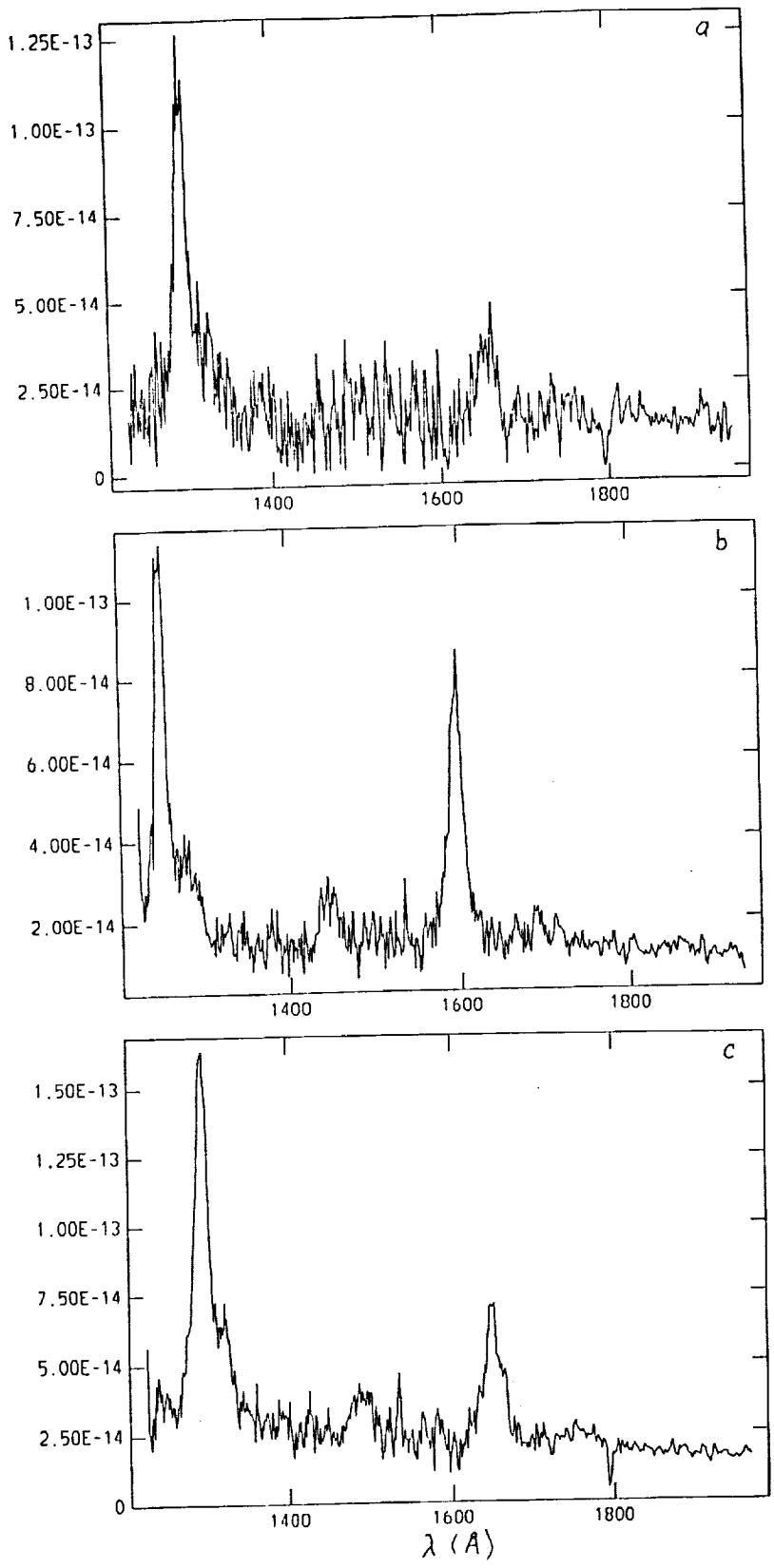
a
1.25E-13
1.00E-13
7.50E-14
5.00E-14
2.50E-14
0
1400
1600
1800
b
1.00E-13
8.00E-14
6.00E-14
4.00E-14
2.00E-14
1400
1600
1800
c
1.50E-13
1.25E-13
1.00E-13
7.50E-14
5.00E-14
2.50E-14
0
1400
1600
1800
λ (A)

Figure 2

PG0844+349

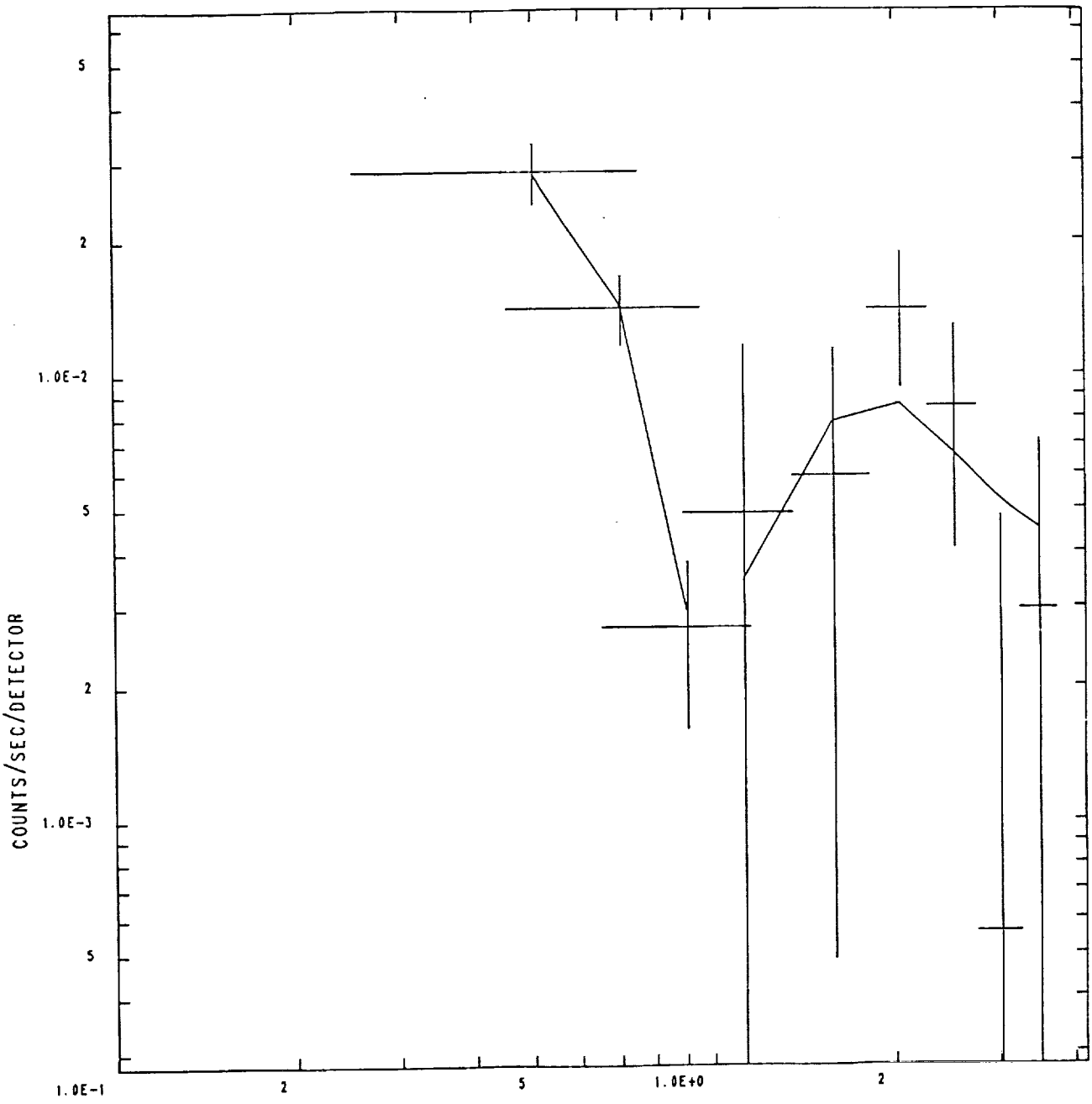

Figure 3

PG0923+129

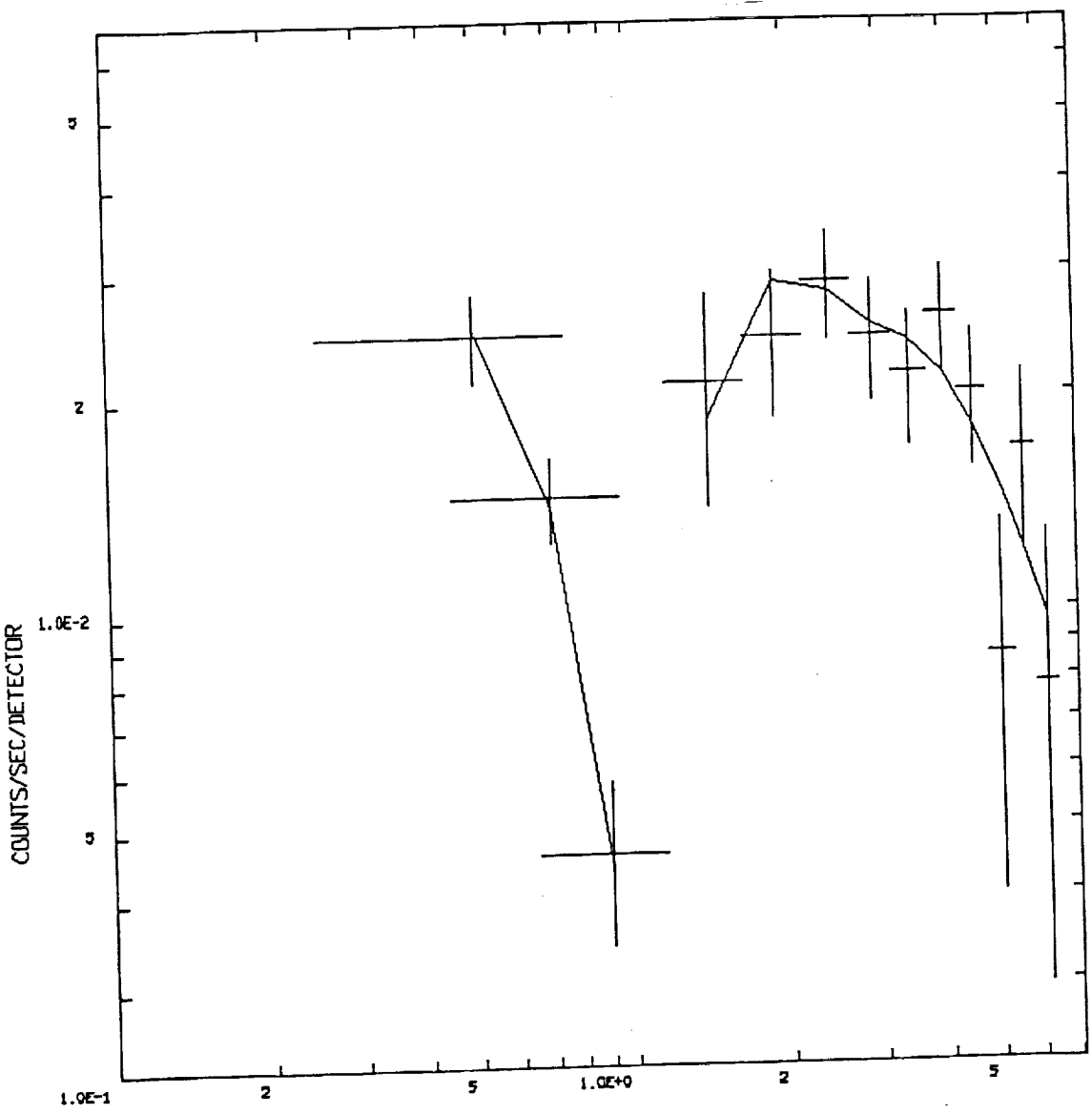

Figure 4

PG1229+204

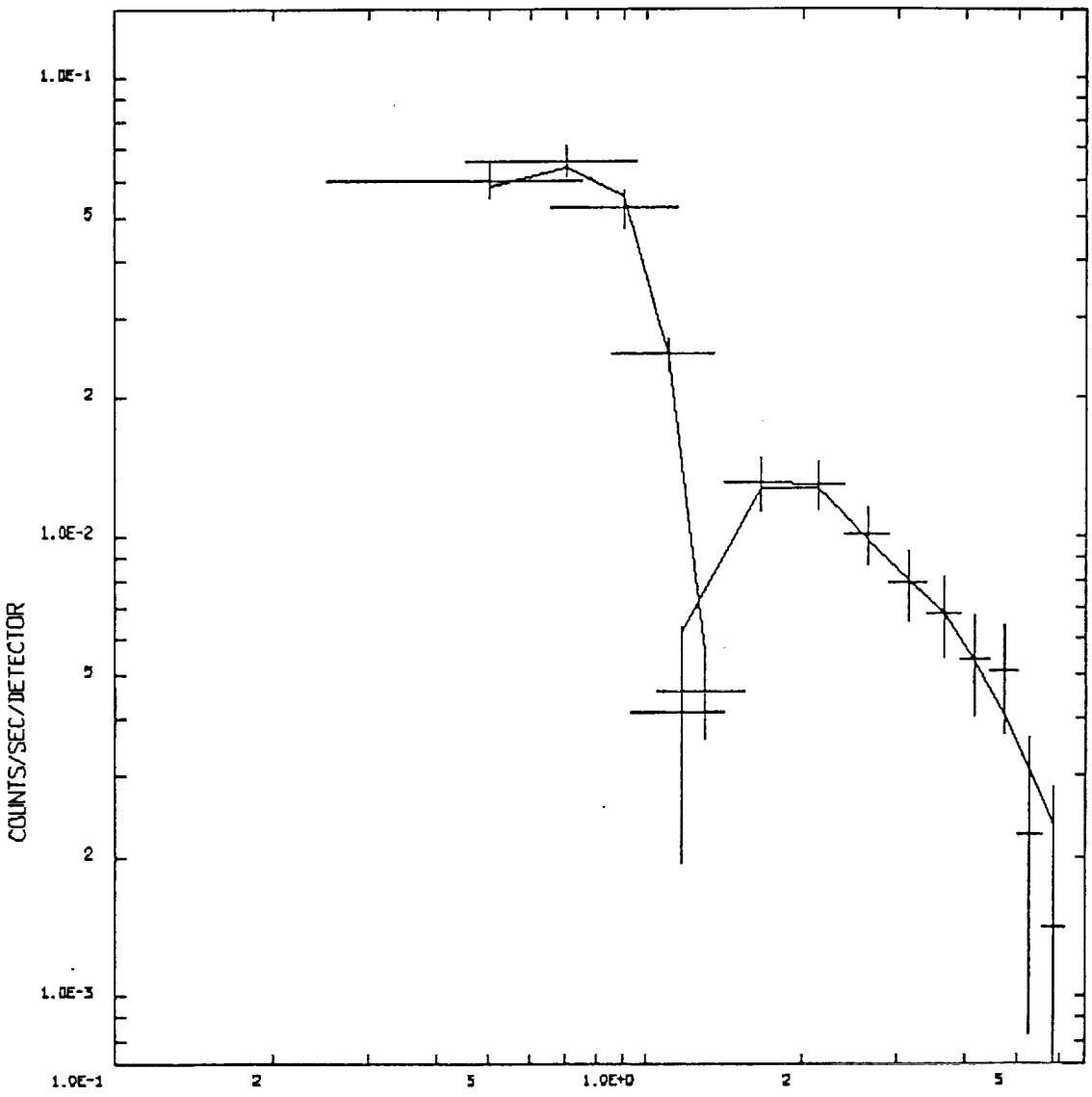

Figure 5

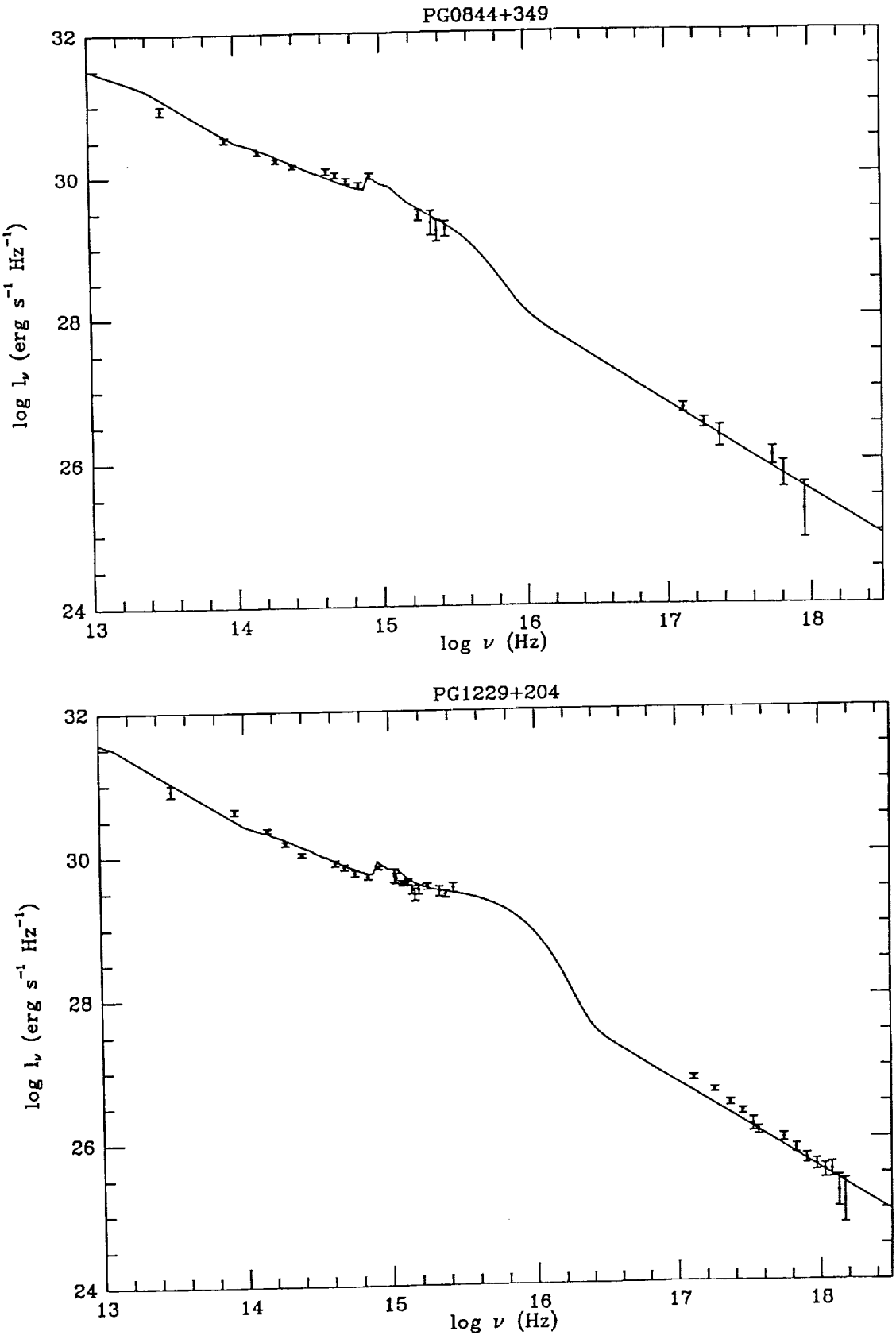
PG0844+349
log l_ν (erg s^{-1} Hz^{-1})
log ν (Hz)
PG1229+204
log l_ν (erg s^{-1} Hz^{-1})
log ν (Hz)

Figure 6